Single Mol. **2** (2001) 4, 261-276

Properties of Fluorescent Semiconductor Nanocrystals and their Application to Biological Labeling

Xavier Michalet [1,2,4], Fabien Pinaud [1,2,4], Thilo D. Lacoste [1,2,5], Maxime Dahan [1,2,6], Marcel P. Bruchez [3,7], A. Paul Alivisatos [1,3] and Shimon Weiss [1,2,4]

[1] *Material Sciences Division , Lawrence Berkeley National Laboratory, 1 Cyclotron Road, Berkeley, CA 94720, USA*

[2] *Physical Biosciences Division, Lawrence Berkeley National Laboratory, 1 Cyclotron Road, Berkeley, CA 94720, USA*

[3] *Department of Chemistry, University of California, Berkeley, CA 94720, USA*

[4] *Department of Chemistry and Biochemistry/Department of Physiology, University of California, Los Angeles, CA 90095, USA*

[5] *Present address:LifeBits AG, Albrechtstr. 9, 72072 Tuebingen, Germany*

[6] *Present address: Laboratoire Kastler Brossel, Ecole Normale Supérieure, 24, rue Lhomond, 75731 Paris Cedex 5, France*

[7] *Present address: Quantum Dot Corp., 26118 Research Road, Hayward, CA 94545, USA*

Correspondence to
Xavier Michalet
Material Sciences Division
Lawrence Berkeley National Laboratory
1 Cyclotron Road, Berkeley, CA 94720, USA
tel +1 (510)-486-4041
fax + 1 (510)-486-5530
email michalet@chem.ucla.edu, sweiss@chem.ucla.edu

submitted 15 Aug 2001
accepted 22 Nov 2001
published 30 Nov 2001

Abstract

We review recent advances in the development of colloidal fluorescent semiconductor nanocrystals (a class of quantum dots) for biological labeling. Although some of the photophysical properties of nanocrystals are not fully understood and are still actively investigated, researchers have begun developing bioconjugation schemes and applying such probes to biological assays. Nanocrystals possess several qualities that make them very attractive for fluorescent tagging: broad excitation spectrum, narrow emission spectrum, precise tunability of their emission peak, longer fluorescence lifetime than organic fluorophores and negligible photobleaching. On the down side, their emission is strongly intermittent ("blinking") and their size is relatively large for many biological uses. We describe how to take advantage of nanocrystals' spectral properties to increase the resolution of fluorescence microscopy measurements down to the nanometer level. We also show how their long fluorescence lifetime can be used to observe molecules and organelles in living cells without interference from background autofluorescence, a pre-requisite for single molecule detectability. Finally, their availability in multicolor species and their single molecule sensitivity open up interesting possibilities for genomics applications.

Introduction

Fluorescent semiconductor nanocystals (NC) properties and applications stands amongst the most exciting research fields in chemistry, physics and biology [1-5]. Their development results from an increasing emphasis put on miniaturization in semiconductor physics. The first step

 1438-5163/01/0211-0261 $ 17.50+.50/0

towards nanometer scale happened in the field of layered semiconductor materials, known as heterostructures. In these two dimensional (2D) geometries [6], the epitaxial growth of precise atomic layers with controlled composition using molecular beam epitaxy [7-9] (MBE) allows to shape and manipulate electronic wavefunctions in the solid at will, giving rise to rich phenomena such as resonant tunneling, integer and fractional quantum Hall effects, quantum confinement, efficient lasing and many more (1973, 1985 and 1998 Nobel Prizes in physics) [10]. The concept of quantum confinement by band-gap engineering of heterostructures was then extended to lower dimensions (1D and 0D) [11]. In the last two decades, we have witnessed tremendous progress in the ability to synthesize quantum wells [12,13], wires [14] and dots [15,16] with high-speed, high-efficiency electronics and optoelectronics devices (information technology) being the main drive.

Quantum confinement arises when one of the dimensions L of the object becomes of the order of the exciton Bohr radius:

$$a_{ex} = \frac{\kappa\hbar^2}{m_{ex}e^2} \quad (1)$$

were κ is the semiconductor permittivity, m_{ex} is the reduced exciton mass, and e the electron charge (for example, a_{CuCl} = 7 Å, a_{GaAs} = 100 Å and a_{CdSe} = 56 Å).

The most useful outcome of quantum confinement for the applications discussed in this paper is the discretization of the energy levels at the edges of the conduction and valence bands upon dimensional reduction. The first controlled synthesis and systematic studies of nanometer size semiconductor crystals in all three dimensions were performed by Ekimov and Éfros [17, 18]. They studied quantum dot inclusions that were embedded in an insulating glass matrix. The same types of material were used long ago, at least since the Middle-Age, in stained glass windows decorating churches with multicolor ornaments. Ekimov's sample was the first to exhibit the quantum-confined blue shift of the first absorption (exciton) peak, varying as a^{-2} (a being the nanocrystal radius) [17]. Solving the effective Hamiltonian for a spherical geometry, Éfros and Éfros computed the electron and hole energies in such a sphere and found a series of discrete lines, recovering the a^{-2} dependency observed in the experiment [18].

Another route to the synthesis of 0D semiconductor structures was explored by several groups, who developed methods for obtaining colloidal particle by diffusion-limited growth in solvents [19-22] (for a review, see ref. [2]). These studies were partly motivated by the mid-seventies energy crisis, which renewed the interest for devices capable of an efficient utilization of solar energy. Colloidal suspensions of semiconductor nanocrystals looked as promising electron or hole donors (catalysts), due to their large surface area to volume ratio [19-21, 23-25]. A side product of these works was the exploration of their luminescent properties, and in particular the relationship between nanocrystal size and fluorescence properties [19,20,22,26]. Continuous improvements have since then been reported [27-31], with a major advance being the addition of different composition, concentric heterostructure layers to the original "core" particle, a concept that was borrowed from "band gap engineering" developed for 2D MBE epitaxial growth [28, 32-36]. This kind of research eventually took preeminence in the field, yielding to today's applications in fluorescent biological labeling [37-42] and possibly tomorrow's applications in tunable lasers [43] and flat panel displays [44-46].

Fluorescence of semiconductor nanocrystals is due to the radiative recombination of an excited electron-hole pair. The resulting ensemble emission spectrum consists mainly of a narrow Lorentzian band, 30-40 nm full width at half maximum (FWHM) slightly Stokes-shifted with respect to the excitation band edge. The absorption spectrum, on the other hand is very broad, and contains quantum confinement features. Both excitation and emission depend on the nanocrystallite size. These spectra are blue-shifted as the nanocrystal diameter is reduced, due to the increase in exciton binding energy. Depending on the material, their spectra can be continuously tuned from the UV-blue (ZnS [47], ZnSe [48]) to near infrared (CdS/HgS/CdS [32, 49], InP, InAs [50, 51]) through the visible (CdE, with E = S, Se, Te [29,52]).

This paper briefly reviews the synthesis and the important photophysical properties of fluorescent semiconductor nanocrystals, which are of interest for their use as biological probes. We describe two applications developed in our lab, multicolor imaging and ultrahigh resolution colocalization that take advantage of these unique photophysical properties. Finally, we review recent examples of biological applications.

Nanocrystal Synthesis

Core Synthesis

Synthesis of semiconductor nanocrystals was initially performed by precipitation from a solution containing the metal ion (Ag, Hg, Pb, Zn, Cd, In) by a hydroxide of S, Se, Te or P, followed by the addition of colloid stabilizers [19,20, 22]. Further progress involved inverse micelle synthesis [27,28] leading to pure and stable powders of organically capped nanocrystals [2]. A further improvement involves high temperature (300 °C), surfactant synthesis starting from dimethyl-cadmium precursors in trioctylphosphine oxide (TOPO). The results are highly monodisperse nanocrystals [29,52]. Recently, a simpler synthesis has been devised using less toxic and reactive cadmium oxide precursors that should allow scaling up the process [53, 54]. The liquid phase is provided by a surfactant (TOPO), which is used together with trioctylphosphine (TOP) to coat

the growing crystallites and prevent their aggregation, as well as limit the dissolution of smaller nanocrystals in favor of larger ones (a process known as Ostwald ripening). The nanocrystallite's size is monitored by removing aliquots of the reaction and checking the absorption spectrum edge, which is a direct signature of the size of the particles [52]. The growth is stopped by cooling down the reaction vial. NCs are then further precipitated to improve their size distribution, and can be dissolved in solvents like butanol, toluene or other non-polar solvents. Particles synthesized this way can have very narrow size distributions, on the order of a few % as shown by high resolution transmission electron microscopy (TEM) [29].

High resolution TEM also shows that these NCs are made of a few hundreds to a few thousands atoms [55], i.e. the surface atoms contribute a non-negligible amount of the total mass. This is where defects are most easily created, and were electrons or holes can be trapped by local potentials.

Shell Synthesis

The quantum yield of "core" NCs is of the order of a few percents only, a rather low value compared to standard organic dyes. The solution borrowed from band gap engineering developed for quantum well heterostructures [6-8], consists in passivating the surface defects (dangling bonds) by growing a lattice-matched, higher band-gap material on top of the nanocrystal core [28, 32,33,35,36]. This "shell" layer serves a double purpose: it eliminates core surface traps and it confines the excitation into the core. CdS (E_g = 2.49 eV) [36] and ZnS (E_g = 3.8 eV) [34, 35] are used as shells for CdSe cores (E_g = 1.75 eV at 300 K). CdS is better lattice-matched to CdSe, but ZnS has a larger band offset [56] and better confinement. Growing a small shell on top of the core dramatically increases the quantum yield, up to values of ~80 %, although more typical values fall around 20-50 %. In addition, the spectra of these "core-shell" NCs are slightly red-shifted with respect to those of the original core NCs due to leaking of the exciton wave function into the shell. Larger shells, however, tend to create strains which reduces the quantum yield.

Solubilization via Silanization

As prepared according to the previous protocols, core and core-shell NCs are soluble in non-polar solvents only. TOPO molecules that are used to prevent aggregation of NCs during synthesis indeed have their aliphatic chains facing the exterior, giving rise to a hydrophobic behavior.

One way to solubilize NCs in water consists of removing the TOPO molecules and replacing them with a linker, which is hydrophobic on one end and hydrophilic on the other. Derivatives of silanes have these combined properties: thiol derivatized silane can be used to prime the surface and form an initial thin layer of silane. Other silane reagents, like aminopropyl-silanes (APS) or phospho-silanes can then be polymerized on top of it via well established silane chemistry. The resulting particles have mercapto (SH) and phosphate groups (PO_4-) or amino (NH_2), groups facing the solution. This ensures solubilization in aqueous buffer and allows further functionalization [37,57,58]. The overall process also leads to polymerization of a silica-like layer around the core-shell NC [37,57,59]. While this protocol has negligible effect on photophysical properties, it significantly enlarges the particles and introduces extra charges on their surface. These charges are useful to prevent aggregation of the nanoparticles. On the other hand, they set an upper limit to the ionic strength of the buffers in which they remain stable and could possibly lead to significant non-specific binding. The size increase may also impede targeting the NCs into crowded nanometer-size cellular compartments. Lastly, the very slow hydrolysis of the silane layer eventually leads to partial precipitation of the NCs, limiting their shelf lifetime.

Other solubilization protocols have been and are still developed. Some of them use thiol (-SH) groups to attach molecules having a carboxyl group (-COOH) available to face the aqueous solution [38,39,60,61]. However, the corresponding link is dynamic, leading to a reduced long-term stability of the nanocrystals. Slow oxidation of the NCs is also possible, degrading their spectral properties.

In summary, solubilization of NCs in aqueous buffer is a domain where much progress is to be expected in the future.

Limiting Photophysical Properties

Undesirable photophysical properties put bounds on the performance of NCs in biological experiments. The most demanding applications will most probably require single NC detectability. Single molecule spectroscopy is therefore the most informative and the tool of choice to reveal the fundamental limitations of this technology. More detailed exposition of NCs photophysics, can be found in recent reviews [2-5].

Emission Spectrum and Spectral Jumps

The ensemble emission spectrum of nanocrystals is rather narrow (30-40 nm) compared to that of standard dyes (see Fig. 1). Also, it is very symmetric, in contrast to conventional dyes that suffer from a long IR vibronic tail. This width actually hides the true atomic-like nature of NCs due to inhomogenous broadening. The homogenous linewidth can only be revealed by single molecule spectroscopy. At cryogenic temperatures, one observes very narrow individual NC emission spectra (width of a few nm or less), with distinguishable longitudinal-optical (LO) phonon side-lines (Fig. 1).

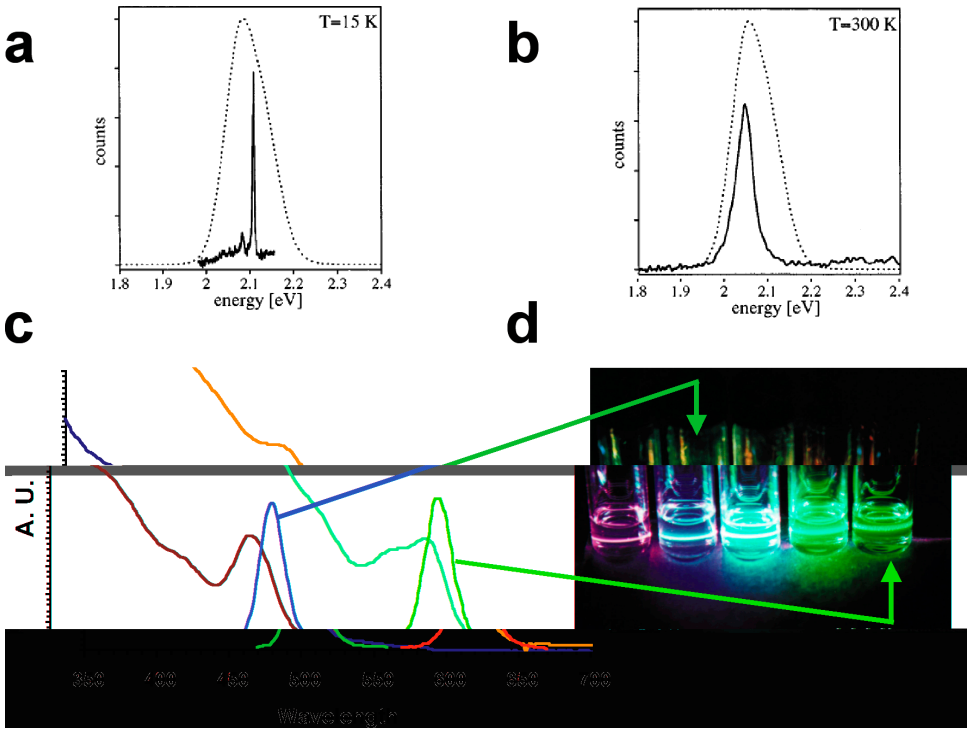

Fig. 1. *Emission spectra.* **a, b:** *Emission spectra of CdSe/CdS core-shell nanocrystals at low temperature (15 K) and room temperature (300 K), respectively (intensity: 1 kW/cm^2, integration time: 60 s). The plain curves correspond to spectra of individual nanocrystals, whereas the dashed curve correspond to bulk spectra. Peak: 2.1 eV = 590 nm. At this wavelength, a width of ΔE = 1 meV corresponds to $\Delta\lambda$ = 0.3 nm. Reproduced from ref. [67].* **c:** *Absorption (violet, blue) and emission (green, red) spectra of two different diameters CdSe/ZnS core-shell nanocrystals, showing the blue shift of both kind of spectra due to quantum confinement of the exciton upon size reduction.* **d:** *Photograph of nanocrystal batches of different emission spectra (i.e. diameters) simultaneously excited with a handheld UV lamp (340 nm). From left to right: 490, 514, 575, 588 and 620 nm. The green and red vials correspond to the spectra shown in c.*

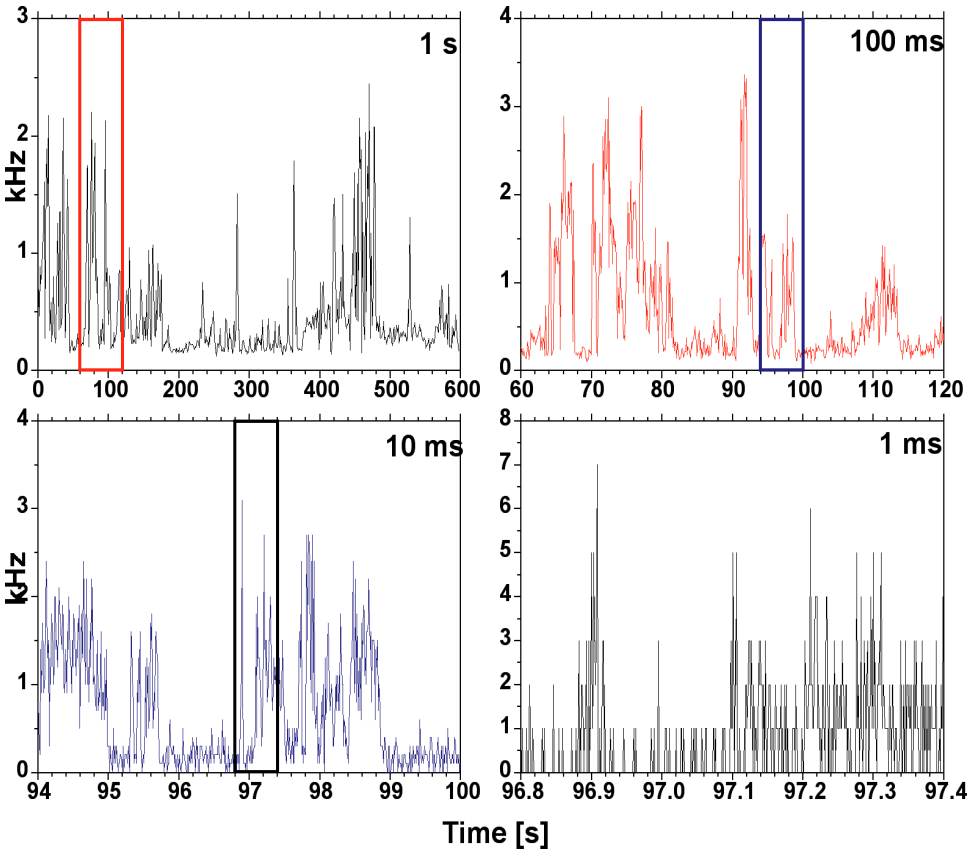

Fig. 2. *Successive zooms of a blinking time trace. Emission intensity of a single CdSe/ZnS nanocrystal excited with a pulsed laser (rep rate: 4.75 MHz) at 460 nm and 1 μW of incident power (x100 oil immersion objective, NA = 1.3) over a period of 10 minutes. Photons were recorded using an avalanche photodiode, whose TTL pulses were recorded by a counting board (see ref. [42, 78] for details on the acquisition setup). Photocounts binning of 1 s allows an overview of the whole time trace. Zooming on shorter time windows (60 s, 6 s, 600 ms) allows smaller binning intervals to be used (100 ms, 10 ms and 1 ms, respectively). The same intermingling of on and off states is visible at all time scales.*

The broadening of the ensemble spectrum is partly due to the size dispersion inherent to the synthesis (inhomogenous broadening) and partly due to spectral jumps (homogeneous broadening). By monitoring an individual NC's spectrum at cryogenic temperatures over several minutes, Empedocles et al discovered shifts of the main peak position ranging from a fraction of a nanometer to several nanometers [62], an observation reproduced under 2-photon excitation [63]. These spectral jumps are likely due to local changes in the NC's environment (or for that matter, on its surface), illustrating again its similarity to molecules, for which these characteristics have been documented [64,65]. Gathering all the recorded emission peaks positions into a histogram recovered the ensemble spectrum.

An interesting consequence of these jumps is that the line width of each individual QD is integration-time dependent, and somewhat more surprisingly, excitation power dependent [66], pointing to a photo-excited mechanism that underlies this phenomenon [67].

Intermittency

More of a surprise, but another illustration of the atomic-like nature of NC is the phenomenon of blinking, first described by Nirmal et al. [68] and rationalized in terms of Auger ionization by Efros and Rosen [69]. This phenomenon is readily observed with a standard fluorescence microscope looking with bare eyes at a diluted solution of NCs spread over a glass coverslip. Individual, bright diffraction-limited spots alternating between an emitting state ("on" or "bright" state) and a non-emitting state ("off" or "dark" state) can easily be observed. This is a very convenient signature of single NC, as this behavior is completely cancelled out when an aggregate of several NC is examined (due to simple statistical considerations).

It is worth looking in more detail to the corresponding intensity fluctuations of a single nanocrystal (Fig. 2), recorded with a single-photon counting detector (avalanche photodiode, APD). The same pattern of on and off times was observed, regardless of the integration (observation) time: the on/off structure of the trace is self-similar [70, 71]. This phenomenon points to a problem in the definition of the quantum yield for a single NC, since it is usually understood that the molecule is in an emitting state [72]. The averaged (observed) ensemble quantum yield is in fact underestimating that of the bright periods, due to their contamination at all time scales by dark periods. If embedded in a protective polymer layer (polymethylmethacrylate, PMMA), NCs can in fact be observed without any noticeable sign of bleaching for up to hours (the limiting factors are the thermal drift of the setup - which puts the NC out of focus – and the large data files generated by such acquisitions) ! The same NC can be repeatedly observed over hours, probably emitting billions of photons. Some of the NCs may eventually become non-emitting, but since very long off time cannot be excluded, and some experiments have shown puzzling recovery effects [73], it may still be premature to speak of photobleaching.

On/Off Time Distributions

A statistical analysis of the on and off times at low temperature shows two effects: one thermal and one related to the excitation intensity [67]. At higher intensity, nanocrystals tend to switch into the off state more often, the averaged off time duration remaining approximately independent of intensity. This can be rationalized by the following Auger ionization model proposed to explain the dark state in nanocrystals [69]: upon each photo-excitation, an electron-hole pair (exciton) is created. In general, it will recombine and emit a Stokes-shifted photon after a typical lifetime of a few dozens nanoseconds. But at high excitation intensity, there is a chance that another electron-hole pair will be created. In general, these extra electron-hole pairs will recombine non-radiatively in several tens of picoseconds [74], but sometimes this recombination will eject one of the carriers of the first pair (say, the electron) by momentum transfer, which might end up being trapped at a surface defect or ejected from the dot (Auger ionization process). As a result, a lone carrier (here a hole) remains in the dot, causing newly formed electron-hole pairs to non-radiatively recombine and leave another lone carrier behind. In some cases, an inverse process can occur either by re-injection of the ejected carrier or by a second ionization that effectively neutralizes the NC (Auger recombination process). In both processes, an increase in off states occurrences is expected at higher excitation intensity: i.e. NCs blink more at higher excitation power.

Interestingly, the distribution of off times is not exponential as would be expected for a thermally controlled deactivation process [68,75], but instead follows a power law dependence with extremely long off times [70,71]. Blinking sets a severe limitation on single NC biological experiments such as tracking and motility assays. It also has noticeable effects in more classical microscopy experiments as shown below.

Correlation Between Spectral Jumps and Blinking

A correlation between spectral jumps and blinking was first observed by Neuhauser et al. at low temperature [76]. The same phenomenon is observed at room temperature as illustrated in Fig. 3. In Fig. 3a, a sample of spin-coated single nanocrystals was raster-scanned using a custom-made confocal microscope [42]. For each position of the sample, a full emission spectrum is recorded (200 nW incident power (380 W/cm^2), 100 ms integration time).

The lines indicated in Fig. 3a are converted to spectra plotted vs. time in Fig. 3b and c: for each pixel in a line scan we obtain a color-coded spectrum that is stacked vertically.

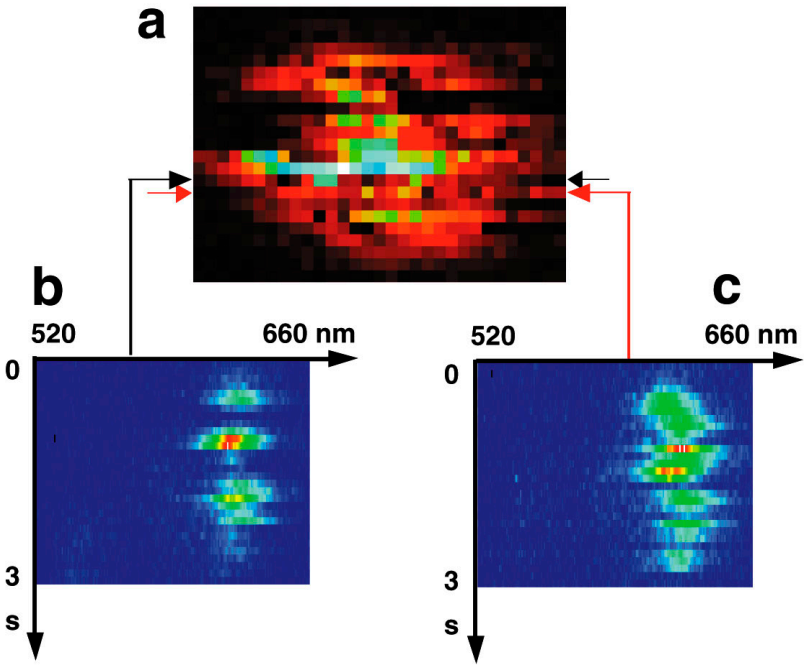

Fig. 3. *Spectral jumps and blinking at RT. A mixture of different CdSe/ZnS NC batches was scanned using a piezo-scanner and excited with a continuous wave (CW) Argon ion laser at 488 nm and 200 nW of incident power (x100 oil immersion, NA = 1.4). For each scanner position, a full spectrum was recorded by an intensified camera as described [42, 78].* **Figure a** *shows part of this scan (pixel size: 23.4 nm, integration per pixel: 100 ms) centered around a single NC emitting at 620 nm.* **Figure b and c** *show a false color representation of the spectra recorded along to successive segments indicated in Figure a (red, yellow and blue correspond to high, medium and low count respectively). Along each segment scan, which takes approximately 3 s, the nanocrystal maps the excitation point spread function (PSF), so that the total intensity first increases to reach a maximum at ~ 1.5 s and decreases afterwards. Superimposed to this intensity modulation, are clear blinking events (blue background), which are accompanied by slight spectral drift or clear spectral jumps. The time resolution of the experiment does not allow to decompose the drifts in series of jumps that probably occur at much shorter time scale.*

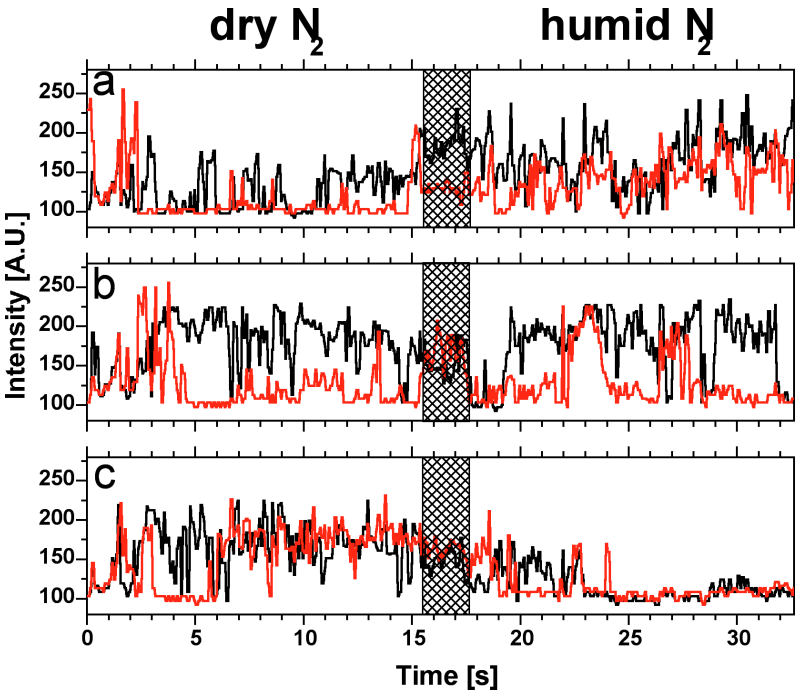

Fig. 4. *Influence of environment. Yellow CdSe/ZnS NCs were observed using a total internal reflection excitation setup allowing simultaneous observation of several individual NCs under controlled environment. Excitation: 1 mW, 488 nm CW Argon ion laser, x63 water immersion objective (NA = 1.2). Detection: intensified camera, integration time: 100 ms. Panels a through c show three different type of behaviors observed for different NCs in the same field of view during a 33 s time window, comprised of two sequences: during the first ~ 15 s, NCs spin-cast on a quartz coverslip were flushed with dry nitrogen; the last ~ 15 s correspond to a humid nitrogen atmosphere obtained by letting the N_2 flow bubble in distilled water. The crossed area indicates fluctuations in intensity and focus subsequent to the flow switch.* **a:** *Decrease of the dark state duration,* **b:** *No marked changes,* **c:** *Increase of the dark state duration. We note that this latter case could also correspond to a genuine "bleaching" of the NCs observable in the absence of environment change.*

Some spectra that show up in background color correspond to regions of the image away from the nanocrystal, whereas some others correspond to off states of the studied NC. The two selected lines show clear blinking correlated with spectral shifts and/or jumps. These spectral jumps have amplitudes of a few nm. This phenomenon has to be very carefully taken into account in single molecule multiplexed assays for correct spectral assignment of adjacent NCs. In fact, this correlation between spectral jumps and blinking can serve as a criteria for the detection of a single NC.

Environment

The photophysical properties of NCs are also strongly dependent on the local environment. Fig. 4 (and Supplementary Material) illustrates the influence of humidity on individual NCs emission. Interaction of water molecules with NCs surface has already been shown to influence the quantum yield of CdSe monolayers on the ensemble level [77]. Here, a sample of spin-coated NCs was mounted in a chamber and observed by total internal reflection (TIR) fluorescence microscopy using an intensified CCD camera. In the first part of the measurement, dry nitrogen was flown into the chamber. In the middle of the sequence, the nitrogen flux was forced to bubble through water, thus yielding a humid nitrogen atmosphere.

As can be observed from 6 different nanocrystals chosen at random, the increased humidity may have a dramatic effect on the emission of some nanocrystals (case a and c), whereas others seem unaffected by the change in environment. This observed diversity illustrates the power of single molecule spectroscopy to distinguish different subpopulations that are mixed up in ensemble measurements [77]. This very crude observation stresses that one should be prepared, in dealing with biological environments, to experience drastic changes in the photophysics of NCs, depending on their local environment. On the other hand, NCs could be devised as very useful indicators of their biological surrounding (that is, when we know enough about environmental effects).

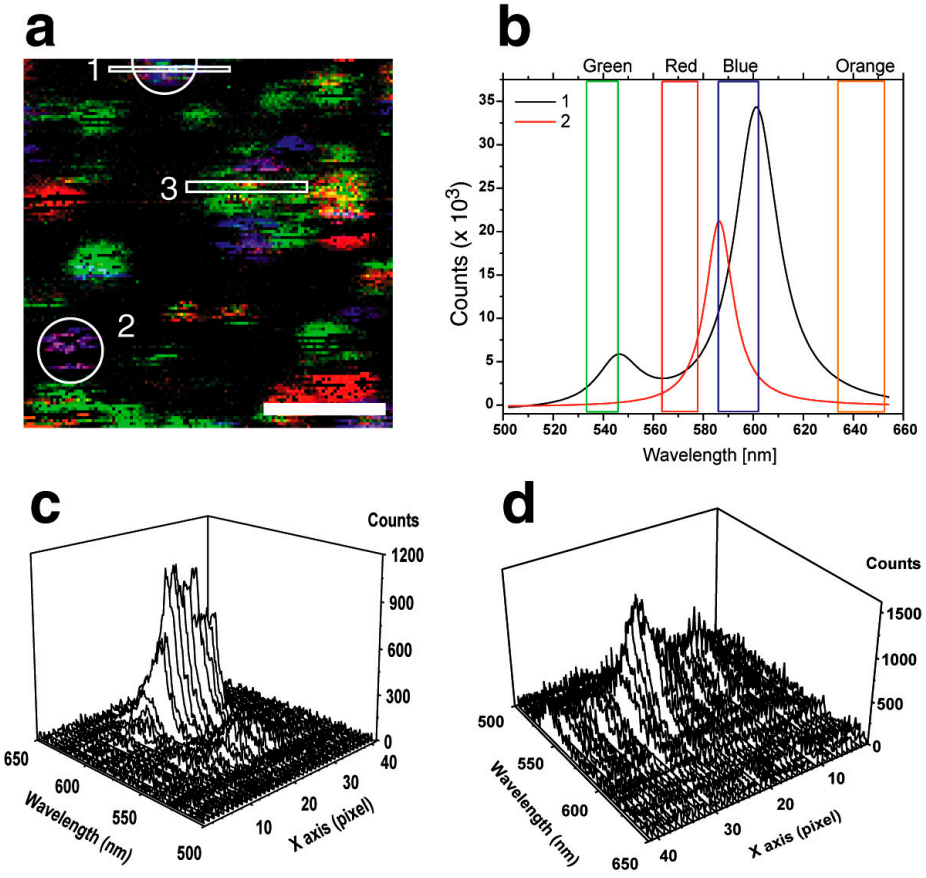

Fig. 5. *Nanocrystals multicolor imaging.* **a:** *3 x 3 μm^2 scan of a mixture of four NC samples (ensemble peak emissions: 540, 575, 588, and 620 nm) obtained as described for Figure 3 (pixel size: 23.4 nm, scale bar: 1 μm).* **b:** *Individual nanocrystal spectra taken at spot 1 and 2 on image a. Digitally defined spectral bands used to construct image a are indicated with their respective false color hue. Spectrum 1 exhibits two peaks indicating the presence of two colocalized nanocrystals.* **c:** *Spectra corresponding to band 1 indicated on image a. The two PSFs corresponding to the two distinct nanocrystal identified in spot 1 are recovered, with the additional information on their respective position (here along the x axis): in this specific case, they are colocalized.* **d:** *Spectra corresponding to band 3 indicated on image a. A wider band has been used to improve the signal-to-noise ratio. Three spectrally overlapping PSFs are distinguishable because of their clear separation along the x axis.*

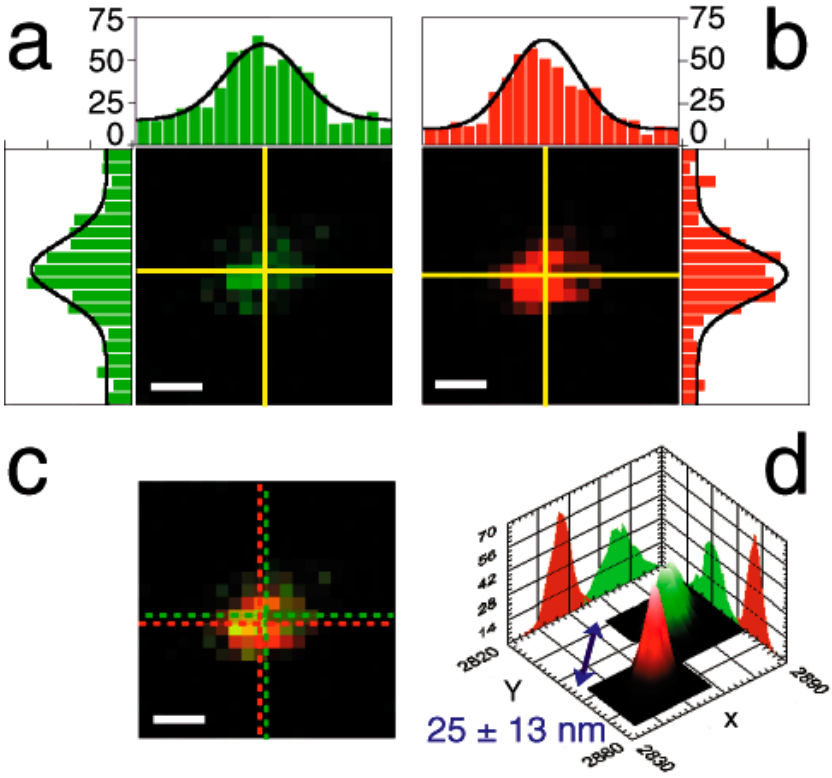

Fig. 6. *Ultrahigh resolution colocalization of individual nanocrystals. Mixture of green (Em: 540 nm) and red (Em: 620 nm) NCs excited at 488 nm (excitation power: 200 nW incident or 320 W/cm^2 peak irradiance, integration time: 50 ms).* **a, b:** *Green and red channel images of a 1 x 1 μm^2 scan obtained by raster scanning the sample through the fixed excitation PSF and recording the respective signals on two different APDs (pixel size: 50 nm, scale bar: 200 nm). As visible from the intensity profiles along two orthogonal lines passing through the PSF's centers, the count rates are similar in both channels. Black curves indicate the corresponding cross-sections of the fitted PSFs.* **c:** *Overlay of the two channels with indication of the determined PSF's centers.* **d:** *Bootstrap replica of the data sets were fitted in order to estimate the uncertainty of the position determination. [84] The figure shows the histograms of the fitted centers distribution obtained from 1000 simulations. The measured distance is 25 nm with a corresponding uncertainty of 13 nm (95 % confidence limit).*

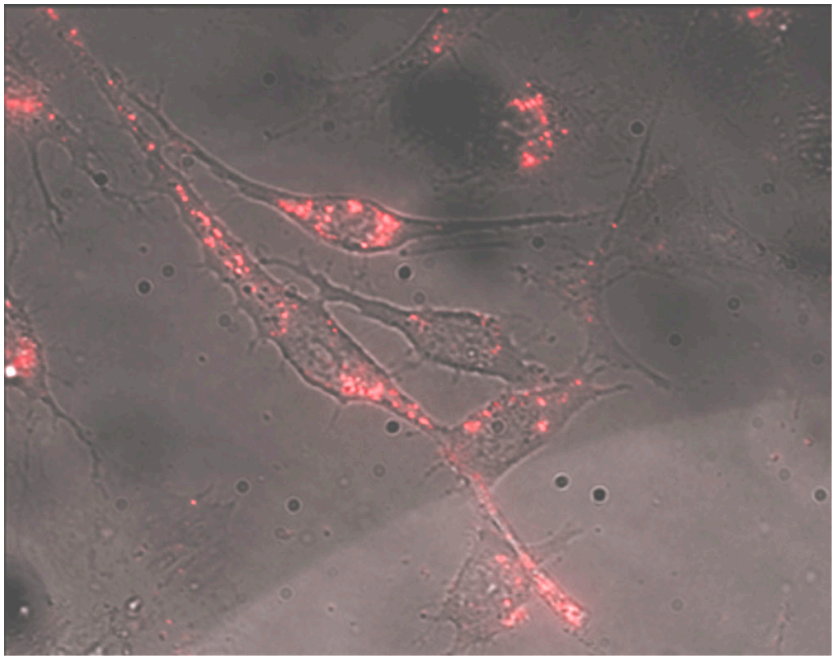

Fig. 7. *Cell Staining. Silanized NCs were added to the growth medium of mouse 3T3 fibroblasts overnight. The medium was then replaced by fresh medium and cells were observed rapidly at room temperature. Overlay of a transmitted light picture of a representative field of view, and the corresponding fluorescence image (mercury lamp illumination, adapted color filter set). The localization of the bright nanocrystals spots is under investigation.*

Taking Advantage of NCs Properties: Multicolor Imaging and Ultrahigh-resolution Colocalization

The properties of NCs can be exploited in unique ways. Below we review several novel methodologies that were developed in our lab.

A detailed description of the custom-made microscopes used in these studies is given elsewhere [42, 78, 79].

A single excitation line is sufficient to excite different NCs above their band edge and have them all emit at their respective wavelengths. This has the obvious advantage that one does not have different chromatic aberrations in the optics of the excitation path, nor does one have to align different excitation beams. We use a stage-scanning confocal set-up with the excitation beam fixed on the optical axis. Nanometer-accuracy positioning is provided by a closed-loop piezo-scanner. An oil-immersion, high NA objective serves both for excitation and collection of the emitted light (epi-illumination).

The simplest detection path we use is composed of two single-photon counting APDs. The signals are spectrally separated using dichroic mirrors and emission filters. While scanning, two separate data sets are recorded simultaneously, and since they result from emission from the same exact point in the sample, they are in perfect registry. The advantage of this configuration is a very high sensitivity and time resolution (in the ns range).

A second type of detection is selected when the number of spectral channels to be monitored is larger than two. This is done by flipping a mirror and redirecting the collected photons to a different path. It would indeed be quite inconvenient to separate multiple colors with multiple dichroic mirrors and detect them with multiple APDs. Instead, the detected photons are dispersed with a Brewster angle prism and imaged onto the photocathode of an intensified CCD camera. The resulting data set consists of a series of spectra, one for each scanned pixel. The temporal resolution of this system is limited to 1 ms, but the noise level and the reduced signal due to the spectral dispersion set a practical limitation of about 50 ms for NC imaging.

Nanocrystal Multicolor Imaging

The narrow emission of NCs permits the preparation of mixture of several NC batches with distinct ensemble spectra. It seems natural to look at the recorded data using our prior knowledge of these ensemble spectra and to define spectral bands that correspond to each individual batch. However, due to overlaps between the ensemble spectra at their tails and due to spectral differences from one NC to another, this approach leads to images that are difficult to interpret.

These problems are illustrated in Fig. 5e digitally defined spectral bands. However, if we go back to the corresponding spectra (Fig. 5b), they correspond to two different situations. In case 1, two distinct spectra are present, each fitting nicely in one predefined spectral band. The multicolor aspect of the spot truly corresponds to different colocalized NCs. On the other hand, case 2 corresponds to a single NC with its spectrum overlapping two spectral bands.

If instead of analyzing the data by predefined bands we utilize the full X-Y-λ data space (or at least at a projection of this space onto the X-λ plane), it is easy to separate NCs that are indistinguishable spatially (they are colocalized), but well separated spectrally (Fig. 5c, case 1); equally well, it is possible to separate NCs that have similar spectra but are well separated in space (> Rayleigh criterion) (Fig. 5d, case 3). Of course in this process, we are ignoring one spatial dimension (Y), which may lift the observed degeneracy in the other dimensions. In conclusion, to fully take advantage of the spectral variety of nanocrystals, some new representation and analysis tools are needed, that go beyond the traditional definition of fixed spectral bands [80].

Nanometer-Resolution Multicolor Colocalization

Another very powerful use of NCs in fluorescence microscopy is taking advantage of their broad excitation spectrum to improve the resolution of distance measurements. Let's consider two spectrally separated nanocrystal batches, spin-coated on a coverslip and observed with the dual channel detection path. The perfect registration of the two channels allows finding out the precise position of each object in the object plane, by fitting the theoretical excitation spot to the observed image [81-83].

It can be shown theoretically, and verified numerically, that for large enough signal-to-noise ratio, and for large enough number of pixels, subpixel accuracy in X and Y can be achieved [81]. In fact, the 2-dimensional fit is even more efficient that a 1-dimensional fit, because there is only one extra parameter (the extra center coordinate), while the number of data points is squared [78]. A crucial ingredient is that the position and size of each pixel be precisely known, achievable with a nm-resolution closed-loop piezo scanner.

As an illustration, Fig. 6 shows a scan of randomly dispersed nanocrystals, observed in conditions were they exhibited moderate blinking. A fit of the respective positions of the overlapping spots gives a distance of approximately 25 nm [42]. The uncertainty in this distance measurement was calculated using the bootstrap method [84]. It yielded a final distance of 25 nm and a "2σ" error bar of 13 nm, comparable to the error bar obtained for non-blinking beads

[42, 79]. Strong blinking significantly affects the reliability of the fit, and a careful analysis of the validity of the bootstrap estimation has in principle to be performed for each blinking statistics. Assuming a power law distribution, it can be shown that the error bar remains reasonably small, even though it is not as good as in the non-blinking case. In any case, the calculated error bar is of the order of the NCs' size, and is therefore close to the best achievable resolution.

Some Examples of Biological Applications of NCs

We now review a few examples of actual use of NCs in a biological context. As a matter of fact, this is a burgeoning field, so that many applications like cell sorting [57], immunoassays [39,40] or fluorescence in situ hybridization [85] among many others [86] will only be evoked here. In addition, we will focus on silanized nanocrystals. Not many of these applications attain the single molecule sensitivity level at this point, but there is no fundamental obstacle to reach this goal in the near future.

Intracellular Staining

The simplest application we can think of is to use these bright fluorescent probes to illuminate the interior of cells. Live cells staining using organic dyes is a well established technique, but unless the cells are loaded with large amount of dye molecules, the stain will eventually bleach due to photophysical degradation. As we have seen, individual NCs have high quantum yields and can emit a very large number of photons, such that a smaller number of probes should be needed to get similar results, reducing the risk of toxicity for the cell. Several methods can be used to load cells with silanized NCs, but certainly the most simple one simply consists of incubating the cells in a medium containing NCs and replacing the medium after a while to wash out the non-incorporated NCs. Surprisingly, this works rather well for 3T3 fibroblasts (see Fig. 7), most likely due to endocytosis of the NCs. In this process, local invaginations of the cell membrane encompass adsorbed NCs into vesicles, which possibly release their cargo in the lysosomes. The exact pathways involved in this uptake process are under investigation.

This proof of principle experiment shows that cells can survive a diet of nanocrystals. Some yeast strains and bacteria do actually much better and synthesize CdS nanocrystals by themselves when placed in a Cd-rich medium [87,88] in an attempt to detoxify their growth medium. The resulting CdS nanocrystals exhibit the same quantum confinement properties as synthetic ones, but tend to degrade upon photoexcitation [89-92].

Functionalization

The next step in cell biology is to target NCs to specific compartments, organelles or molecules. A classical example of these affinity pairs is the biotin-streptavidin pair. Biotin (vitamin) is a small molecule, whereas streptavidin is a 60 kDa protein that can afford to bind up to 4 biotins. Taking advantage of either the NH_2 or SH groups left by amino-propyl silane or mercapto-propyl silane on the surface of silanized NCs, it is possible to use commercially available reactive biotin molecules and covalently attach them on the surface of NCs [57]. The efficiency of biotinylation can be checked by gel shift assay, whereby the migration of a sample of free biotinylated NCs under electric field is compared to that of the same sample mixed with increasing quantities of streptavidin. Whereas singly biotinylated NCs migrate up to a certain point as a relatively narrow band, this band slows down upon addition of streptavidin, which is a signature of the probe's activity (attachment to streptavidin). If more biotins are attached onto each NC during functionalization, one expects that either several streptavidin will bind to each single NC, or that a single streptavidin may cross-link two biotinylated NCs, slowing down even further the migration of the band in the gel. The experiments fully confirm this picture and similar strategies can be used to attach nanocrystals to antibodies or other molecules, and the same sort of test is used to demonstrate specificity.

Fixed Cell Labelling

The first example of specific labeling was obtained early using this simple strategy of biotin functionalization of NCs as illustrated in Fig. 8 [37]. Using cells that were fixed (essentially plasticized) and incubated with biotinylated phalloidin that binds to F-actin filaments, the cytoskeleton was decorated with biotins. Then streptavidin was added, and bound to the biotins present on the filaments. The next step consisted, after rinsing off all the unattached streptavidins, in incubation with the biotinylated NCs, which bound to one of the 3 remaining binding sites of the streptavidins. This type of "sandwich" labeling scheme was repeated once to increase the signal's brightness. A positively charged species of green NCs was added and turned out to bind preferentially within the nucleus. This colorful picture is nothing extraordinary for cell biologists who are used to multicolor, specific staining of different organelles or molecules with organic dyes, but it was an encouraging step towards more ambitious goals. In particular, it was taken using a single excitation source for both colors simultaneously.

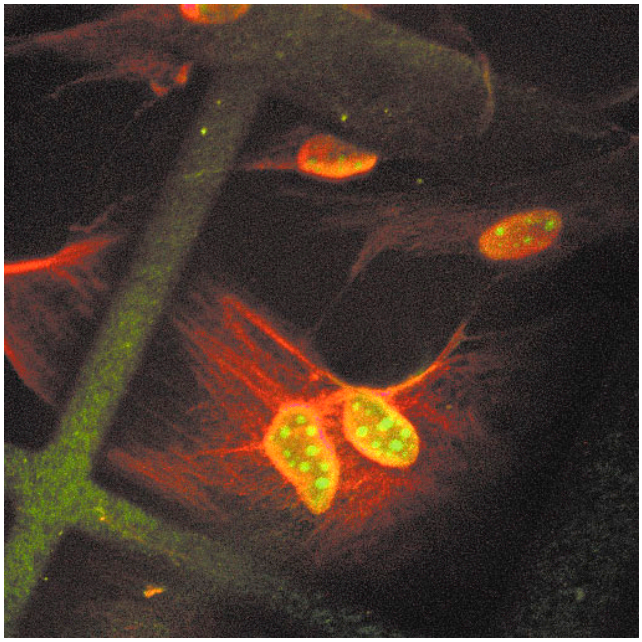

Fig. 8. *Specific actin labeling. Dual-labeled sample examined with a Bio-Rad 1024 MRC laser-scanning confocal microscope with an oil immersion objective (NA = 1.3). Mouse 3T3 fibroblasts were grown on fibronectin-treated, formvar-coated gold grids, and prepared as described in ref. [37]. Briefly, biotinylated phalloidin was incubated with the fixed cell to allow for actin recognition. At the same time, unbiotinylated green NC were added in the detection medium. Biotin was then detected by streptavidin after washing out the unbound phalloidin by rinsing. After washing out the unbound streptavidin, biotinylated red NC were used to detect streptavidin. This double detection layer (streptavidin, biotinylated red NC) was applied twice to increase the contrast. A false-colored image was obtained with 363 nm excitation and simultaneous two-channel detection (522DF35 narrow-pass filter for the green, and a 585 nm long-pass filter for the red). Red NCs are clearly outlining the actin cytoskeleton fibers, whereas the green NCs have non-specifically bound to the nucleus. Field dimension: ~100 μm. The gold grid can be seen in the green channel, most likely due to some bleed-through of the scattered excitation source.*

Time-Gated Imaging of Cells

Another domain where NCs have clear advantages over conventional dyes is the time domain.

We have briefly mentioned above the relatively long fluorescence lifetime of NCs. Ensemble measurements show a multi-exponential decay after pulsed excitation, which gives decay times between 10 and 40 ns [41, 72]. This is much longer than typical dyes or autofluorescent flavin proteins, which have decay times on the order of a few ns. In fact, even without staining, autofluorescence of several proteins often precludes observation of minute details if the target is not heavily loaded with many dyes (which in turn results in phototoxicity problems). If, however, one takes advantage of the long lifetime of NCs and uses pulsed laser excitation, it is possible to reject all photons emitted within the first few ns after the pulse, and keep only those arriving after all dye or autofluorescent proteins have emitted there very last photon (time-gated imaging). Compared to even longer-lived systems like metal-ligand complexes (μs) [93] or luminescent lanthanides (ms) [94], nanocrystals still allow a repetition rate of a few megahertz compatible with rapid cell imaging.

In Fig. 9a live 3T3 cells were incubated with silanized NCs as previously described, and were fixed before observation. Part of the autofluorescence of the cell is in fact due to the fixation process. In any case, even if some bright spots are detectable, it is very hard to distinguish background from genuine signal. Fig. 9b shows the processed image after rejecting all photons emitted within the first 35 ns after each laser pulse, and keeping those emitted between 35 ns until 65 ns after the laser pulse. The background has totally disappeared, leaving only a few bright spots corresponding to the localization of clusters of nanocrystals. The gain in signal-to-background ratio is 15. In spite of rejecting valuable photons, a great enhancement in sensitivity is achieved. It is quite possible that individual NCs in cells could be detected in this manner.

Since the spectral information is not lost, it should be possible to combine spectral information with time-gated detection to localize different NCs in the cell, background-free. This would be even more efficient in live cells, where the autofluorescence is reduced.

Gene Physical Mapping Studies

There has been a tremendous effort in the past decade to decipher the human genome sequence. It is very likely that many approaches in genetics will become obsolete. However, many questions will be answered not by a full-small genome sequencing, but rather by small analysis of local regions. This is especially true in genetic diagnostics and studies of genome rearrangement.

Before a more specific discussion is given, we need to briefly introduce a technique dubbed "molecular combing". This method consists, after extraction of the DNA from cells, in putting it in a buffer solution at pH 5.5, and dipping in an hydrophobic glass surface. After specific binding of DNA molecules by their extremities only, removal of the glass slide out of the solution leads to a gentle stretching of the molecules by the meniscus, which end-up aligned parallel to one another [95-98]. Since the meniscus exerts a constant force on the molecules, they are stretched with a constant factor, which corresponds to 2000 base pairs (2 kb) per measured micrometer of DNA.

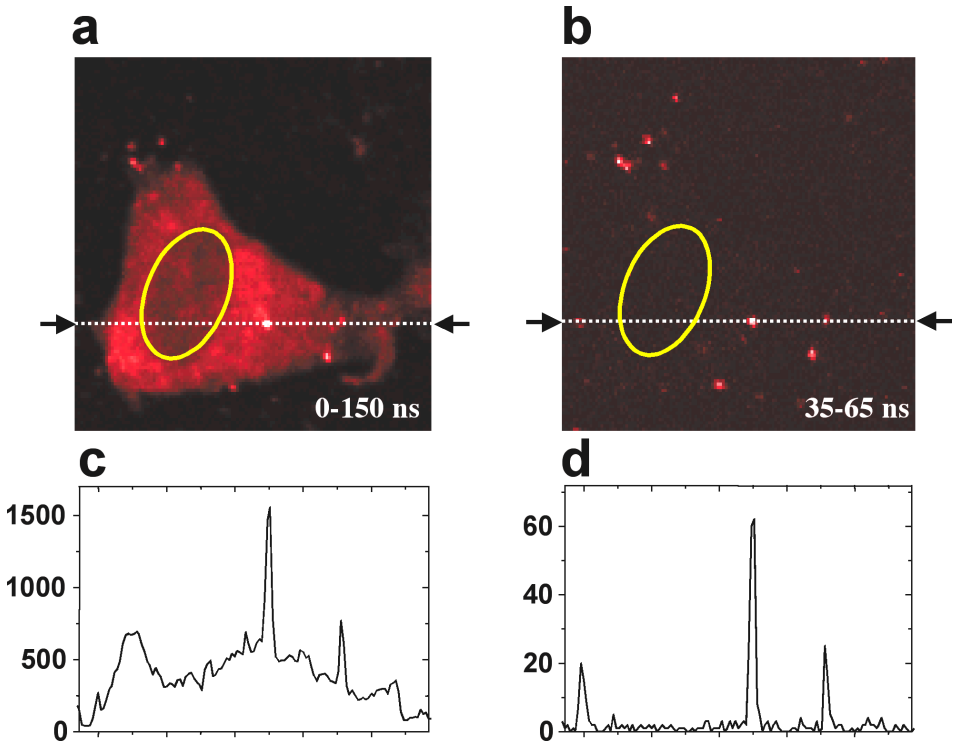

Fig. 9. *Time-Gated Imaging.* **a:** *Mouse 3T3 fibroplasts were incubated with NCs as describe for Figure 7 and fixed in 2 % formaldehyde, 0.5 % glutaraldehyde. Observations were performed with a homemade confocal microscope (for details see ref. [41]). Integration time per pixel is 10 ms, the lifetime window being 0-150 ns after the laser pulse (repetition rate: 5 MHz): this image is obtained using all the detected photons). The ellipse indicates the location of the nucleus.* **b:** *The same recording, but retaining only photons arrived between 35 and 65 ns after a laser pulse. A marked decrease of the background is observed, with a few bright spots clearly dominating.* **c and d:** *Intensity profiles along the white dashed line in a and b. The total signal decreases notably, but the signal to average background ratio jumps from 3 to 45. Note that part of the cytoplasm fluorescence is probably due to NCs too.*

This sort of preparation provides a DNA template, with hundreds of copies of the human genomes per coverslip. Using standard techniques of DNA hybridization and fluorescent detection, it was for instance possible to visually demonstrate deletions of large or small parts of the genome in some genetic diseases, with a precision of a few thousand base pairs [98]. The resolution of this measurement is the best available, and is partly limited by the stretching factor dispersion, but mainly by the optical resolution. An increase in resolution would certainly open new opportunities for discoveries. We have seen how to break the diffraction limit by taking advantages of the NCs properties, and showed that we could measure distances of the order of 20 nm with an accuracy of the order of 10 nm. This would translate into distances of 40 base pairs and an accuracy of 20 base pairs.

Steps have been made towards this goal. We have in particular proven that this hybridization scheme works, as illustrated in Fig. 10, showing the result of a full λ-DNA biotinylated probe hybridized on λ-DNA molecules, and detected with the streptavidin + biotinylated NC sandwich approach [57]. There are a few steps remaining to study small pieces of genome (like transposons, cDNA, inserted viral sequences, etc). These sequences are of the order of a few hundred base pairs. Their respective orientation could conveniently be detected by labeling their ends with NCs of different colors. Their sizes and distances could be measured with a precision of about 20 base pairs. This will probably require using oligonucleotide-functionalized NCs in order to have end-specific labeling of the studied sequences [85].

An important application of this approach would arise from combining this DNA fluorescent tagging with the colocalization of DNA-binding proteins. This constitutes part of the next step in the exploration of the human genome: what do all the expressed proteins do, and how do they interact? Since proteins tightly regulate the dynamics of gene expression, it is extremely important to know which protein participate in this regulation, and if this performed by DNA binding, what are the binding sites. This could be possibly assessed using either purely NCs based gene fluorescence studies (by protein labeling), or a combination of fluorescence (for DNA) and AFM imaging (for proteins).

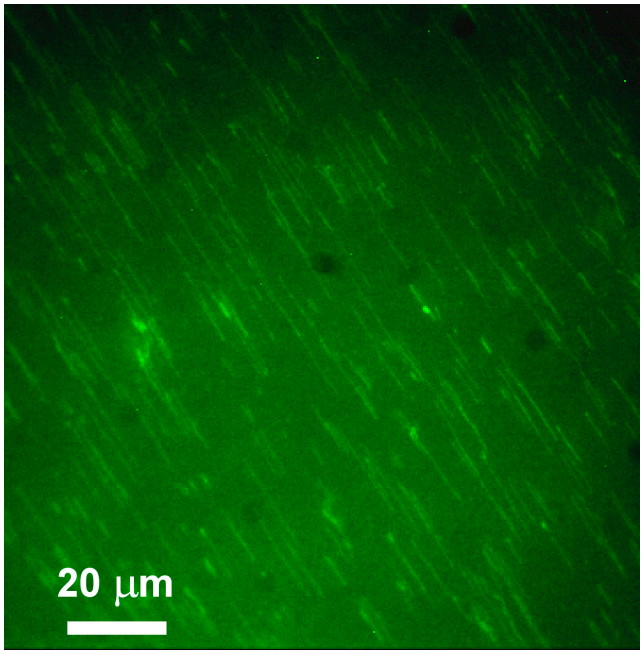

Fig. 10. *DNA combing stained with NCs. λ-DNA in 50 mM MES buffer was combed on silanized coverslip as described in ref. [98]. Biotinylated λ-DNA probes were prepared by random priming and hybridized to the combed DNA as described [98]. A first layer of streptavidin was used for detection (20 μg/ml, incubation 20 min at 37 °C), followed by 3 times 3 min rinsing in 4x SSC (Saline Sodium Citrate), 0.01 % Tween-20. A final layer of biotinylated NC was used detection (incubation 20 min at 37 ºC), followed by a series of 3 rinsing steps in PBS (Phosphate Buffered Saline). The sample was then mounted in 10 % glycerol in PBS under a clean coverslip and sealed with nail polish for further observation. Observation was performed using a standard epifluorescence microscope (mercury lamp, adapted filter set), and images acquired using a cooled CCD camera (10 seconds integration time). The observed fiber size corresponds to the expected stretched λ-DNA molecule size (24 μm).*

Conclusion and Perspectives

In summary, we have discussed some basic photophysical properties of fluorescent semiconductor nanocrystals, which are of interest for their practical use as biological probes, and provided a few illustrations of actual biological applications of nanocrystals. While NCs are still far from being able to fulfill the dream of any biologist, which is to be able to visualize biological reactions taking place in vivo, with the very much needed nanometer resolution, they will undoubtedly play an important role in cellular studies using multicolor labeling, high-resolution localization and time-gated detection.

Nanocrystals will not replace conventional dyes or GFP-tagged recombinant proteins that have pervaded biology. They will serve as an additional, perfectible instrument added to the biologist's or biophysicist's toolbox. A number of studies remain to be done to better understand photophysical properties of nanocrystals in different environments, and hopefully improve them, notably as far as blinking is concerned. Encouraging results in NC's functionalization just begin to flourish and this constitutes one of the most promising research avenues for biological applications. Finally, their tunability and availability in different spectral range will certainly require some technological adaptation in terms of detector technology and novel instrumentation. In any case, they are very likely to continue to fascinate physicists, chemists and biologists for quite some time.

Acknowledgment: This article is based on the work of several collaborators: Uri Banin, Taekjip Ha, Mario Moronne, Rodolphe Hoppeler. We thank Donna Hamamoto for help with the 3T3 cell cultures. Cheryl Weisenmiller was of inappreciable help in providing numerous references from the literature. D. S. Chemla's support over the years is deeply appreciated. Part of this work was funded by the National Institutes of Health, National Center for Research Resources, Grant No. 1 R01 RR1489101, and by the U.S. Department of Energy under Contract No. DE-AC03-76SF00098. X. M. benefited from a Human Frontier Science Program Postdoctoral Fellowship. M. P. B. was supported by a NSF Graduate Research Fellowship.

References

[1] A. P. Alivisatos, Science **271** (1996) 933-937.
[2] L. Brus, Journal of Physical Chemistry of Solids **59** (1998) 459-465.
[3] S. Empedocles, M. Bawendi, Accounts in Chemical Research **32** (1999) 389-396.
[4] M. Nirmal, L. Brus, Accounts in Chemical Research **32** (1999) 407-414.
[5] A. L. Efros, M. Rosen, Annual Review of Material Science **30** (2000) 475-521.
[6] L. Esaki, R. Tsu, IBM Journal of Research and Development (1970) 61-65.
[7] A. Y. Cho, Applied Physics Letters **19** (1971) 467-468.

[8] R. Dingle, A. C. Gossard, H. L. Stormer, Bell Laboratories Record **58** (1980) 274-281.
[9] A. C. Gossard, IEEE Journal of Quantum Electronics QE-**22** (1986) 1649-1655.
[10] L. Esaki, IEEE Journal of Quantum Electronics QE-**22** (1986) 1611-1624.
[11] Y. Arakawa, H. Sakaki, Applied Physics Letters **40** (1982) 939-941.
[12] R. Dingle, W. Wiegmann, C. H. Henry, Physical Review Letters **33** (1974) 827-830.
[13] R. C. Miller, D. A. Kleinman, W. T. Tsang, A. C. Gossard, Physical Review B **24** (1981) 1134-1136.
[14] P. M. Petroff, A. C. Gossard, R. A. Logan, W. Wiegmann, Applied Physics Letters **41** (1982) 635-638.
[15] Y. Arakawa, A. Yariv, IEEE Journal of Quantum Electronics QE-**22** (1986) 1887-1899.
[16] M. Asada, Y. Miyamoto, Y. Suematsu, IEEE Journal of Quantum Electronics QE-**22** (1986) 1915-1921.
[17] A. I. Ekimov, A. A. Onuschenko, Sov. Phys. Semicond. **16** (1982) 775-778.
[18] A. L. Efros, A. L. Efros, Sov. Phys. Semicond. **16** (1982) 772-775.
[19] D. Duonghong, J. Ramsden, M. Grätzel, Journal of the American Chemical Society **104** (1982) 2985-2988.
[20] A. Henglein, Journal of Physical Chemistry **86** (1982) 2291-2293.
[21] J. Kuczynski, J. K. Thomas, Chemical Physics Letters **88** (1982) 445-447.
[22] R. Rossetti, L. Brus, Journal of Physical Chemistry **86** (1982) 4470-4472.
[23] G. Hodes, J. Manassen, D. Cahen, Nature **261** (1976) 403-404.
[24] B. Miller, A. Heller, Nature **262** (1976) 680-681.
[25] L. E. Brus, Journal of Chemical Physics **79** (1983) 5566-5571.
[26] A. Fotjik, H. Weller, U. Koch, A. Henglein, Ber. Bunsenges. Phys. Chem. **88** (1984) 969-977.
[27] M. L. Steigerwald, A. P. Alivisatos, J. M. Gibson, T. D. Harris, R. Kortan, A. J. Muller, A. M. Thayer, T. M. Duncan, D. C. Douglass, L. E. Brus, Journal of the American Chemical Society **110** (1988) 3046-3050.
[28] A. R. Kortan, R. Hull, R. L. Opila, M. G. Bawendi, M. L. Steigerwald, P. J. Carroll, L. E. Brus, Journal of the American Chemical Society **112** (1990) 1327-1332.
[29] C. B. Murray, D. J. Norris, M. G. Bawendi, Jounal of the American Chemical Society **115** (1993) 8706-8715.
[30] X. Peng, J. Wickham, A. P. Alivisatos, Journal of the American Chemical Society **120** (1998) 5343-5344.
[31] L. Manna, E. C. Scher, A. P. Alivisatos, Journal of the American Chemical Society **122** (2000) 12700-12706.
[32] A. Eychmüller, A. Mews, H. Weller, Chemical Physics Letters **208** (1993) 59-62.
[33] A. Mews, A. Eychmüller, M. Giersig, D. Schoos, H. Weller, Journal of Physical Chemistry **98** (1994) 934-941.
[34] M. A. Hines, P. Guyot-Sionnest, Journal of Physical Chemistry **100** (1996) 468-471.
[35] R. O. Dabbousi, J. Rodriguez-Viejo, F. V. Mikulec, J. R. Heine, H. Mattoussi, R. Ober, K. F. Jensen, M. G. Bawendi, Journal of Physical Chemistry B **101** (1997) 9463-9475.
[36] X. Peng, M. C. Schlamp, A. V. Kadavanich, A. P. Alivisatos, Journal of the American Chemical Society **119** (1997) 7019-7029.
[37] M. Bruchez, M. Moronne, P. Gin, S. Weiss, A. P. Alivisatos, Science **281** (1998) 2013-2015.
[38] W. C. W. Chan, S. Nie, Science **281** (1998) 2016-2018.
[39] H. Mattoussi, J. M. Mauro, E. R. Goldman, G. P. Anderson, V. C. Sundar, F. V. Mikulec, M. G. Bawendi, Journal of the American Chemical Society **122** (2000) 12142-12250.
[40] B. Sun, W. Xie, G. Yi, D. Chen, Y. Zhou, J. Cheng, Journal of Immunological Methods **249** (2001) 85-89.
[41] M. Dahan, T. Laurence, F. Pinaud, D. S. Chemla, A. P. Alivisatos, M. Sauer, S. Weiss, Optics Letters **26** (2001) 825-827.
[42] T. D. Lacoste, X. Michalet, F. Pinaud, D. S. Chemla, A. P. Alivisatos, S. Weiss, Proceedings of the National Academy of Sciences USA **97** (2000) 9461–9466.
[43] V. I. Klimov, A. A. Mikhailovsky, S. Xu, A. Malko, J. A. Hollingsworth, C. A. Leatherdale, H.-J. Eisler, M. G. Bawendi, Science **290** (2000) 314-317.
[44] B. O. Dabbousi, M. G. Bawendi, O. Onitsuka, M. F. Rubner, Applied Physics Letters **66** (1995) 1316-1318.
[45] V. Colvin, M. Schlamp, A. P. Alivisatos, Nature **370** (1994) 354-357.
[46] C. Wang, M. Shim, P. Guyot-Sionnest, Science **291** (2001) 2390-2392.
[47] H. Weller, U. Koch, M. Gutiérrez, A. Henglein, Berichte der Bunsengesellschaft Physical Chemistry **88** (1984) 649-656.
[48] M. A. Hines, P. Guyot-Sionnest, Journal of Physical Chemisry B **102** (1998) 3655-3657.
[49] A. Mews, A. Eychmûller, Berichte der Bunsengesellschaft. Physical Chemistry **102** (1998) 1343-1357.
[50] A. A. Guzelian, J. E. B. Katari, A. V. Kadavanich, U. Banin, K. Hamad, E. Juban, A. P. Alivisatos, R. H. Wolters, C. C. Arnold, J. R. Heath, Journal of Physical Chemistry **100** (1996) 7212-7219.
[51] A. A. Guzelian, U. Banin, A. V. Kadavanich, X. Peng, A. P. Alivisatos, Applied Physics Letters **69** (1996) 1432-1434.

[52] J. E. B. Bowen Katari, V. L. Colvin, A. P. Alivisatos, Journal of Physical Chemistry **98** (1994) 4109-4117.
[53] Z. A. Peng, X. Peng, Journal of the American Chemical Society **123** (2001) 183-184.
[54] L. Qu, A. Peng, X. Peng, Nanoletters **1** (2001) 333-337.
[55] A. Kadavanich, V., T. C. Kippeny, M. M. Erwin, S. J. Pennycook, S. J. Rosenthal, Journal of Physical Chemistry B **105** (2001) 361-369.
[56] K. W. Böer, Survey of Semiconductor Physics. Electrons and Other Particles in Bulk Semiconductors, Van Nostrand Reinhold, New York 1990.
[57] M. Bruchez, PhD Thesis, Department of Chemistry, UC Berkeley, Berkeley 1998.
[58] D. Gerion, F. Pinaud, S. C. Williams, W. J. Parak, D. Zanchet, S. Weiss, A. P. Alivisatos, Journal of Physical Chemistry B (2001) 8861-8871.
[59] M. A. Correa-Duarte, M. Giersig, L. M. Liz-Marzán, Chemical Physics Letters **286** (1998) 497-501.
[60] C. C. Chen, C. P. Yet, H. N. Wang, C. Y. Chao, Langmuir **15** (1999) 6845.
[61] G. P. Mitchell, C. A. Mirkin, R. L. Letsinger, Journal of the American Chemical Society **121** (1999) 8122-8123.
[62] S. A. Empedocles, D. J. Norris, M. G. Bawendi, Physical Review Letters **77** (1996) 3873-3876.
[63] S. A. Blanton, M. A. Hines, P. Guyot-Sionnest, Applied Physics Letters **69** (1996) 3905-3907.
[64] M. Orrit, J. Bernard, Physical Review Letters **65** (1990) 2716-2719.
[65] W. P. Ambrose, W. E. Moerner, Nature **349** (1991) 225-227.
[66] S. A. Empedocles, M. G. Bawendi, Journal of Physical Chemistry **103** (1999) 1826-1830.
[67] U. Banin, M. Bruchez, A. P. Alivisatos, T. Ha, S. Weiss, D. S. Chemla, Journal of Chemical Physics **110** (1999) 1195-1201.
[68] M. Nirmal, B. O. Dabbousi, M. G. Bawendi, J. J. Macklin, J. K. Trautman, T. D. Harris, L. E. Brus, Nature **383** (1996) 802-804.
[69] A. L. Efros, M. Rosen, Physical Review Letters **78** (1997) 1110-1113.
[70] M. Kuno, D. P. Fromm, H. F. Hamann, A. Gallagher, D. J. Nesbitt, Journal of Chemical Physics **112** (2000) 3117-3120.
[71] K. T. Shimizu, R. G. Neuhauser, C. A. Leatherdale, S. A. Empedocles, W. K. Woo, M. G. Bawendi, Physical Review B **63** (2001) 205316.
[72] B. Lounis, H. A. Bechtel, D. Gerion, A. P. Alivisatos, W. E. Moerner, Chemical Physics **329** (2000) 399-404.
[73] B. C. Hess, I. G. Okhrimenko, R. C. Davis, B. C. Stevens, Q. A. Schulzke, Q. A. Wright, C. D. Bass, C. D. Evans, S. L. Summers, Physical Review Letters **86** (2001) 3132-3135.
[74] V. I. Klimov, A. A. Mikhailovsky, D. W. McBranch, C. A. Leatherdale, M. G. Bawendi, Science **287** (2000) 1011-1013.
[75] J. Tittel, W. Göhde, F. Koberling, A. Mews, A. Kornowski, H. Weller, A. Eychmüller, T. Basché, Berichte der Bunsengesellschaft Physical Chemistry **101** (1997) 1626-1630.
[76] R. G. Neuhauser, K. T. Shimizu, W. K. Woo, S. A. Empedocles, M. G. Bawendi, Physical Review Letters **85** (2000) 3301-3304.
[77] S. R. Cordero, P. J. Carson, R. A. Estabrook, G. F. Strouse, S. K. Buratto, Journal of Physical Chemistry B **104** (2000) 12137-12142.
[78] X. Michalet, T. D. Lacoste, S. Weiss, Methods **25** (2001) 87-102.
[79] X. Michalet, T. D. Lacoste, F. Pinaud, D. S. Chemla, A. P. Alivisatos, S. Weiss, SPIE Proceedings **4358** (2001). 8-15
[80] D. H. Burns, J. B. Callis, G. D. Christian, E. R. Davidson, Applied Optics **24** (1985) 154-161.
[81] N. Bobroff, Review of Scientific Instruments **57** (1986) 1152-1157.
[82] E. Betzig, Optics Letters **20** (1995) 237-239.
[83] T. Ha, T. Enderle, D. S. Chemla, S. Weiss, IEEE Journal of Selected Topics in Quantum Electronics **2** (1996) 1115-1128.
[84] B. Efron, R. J. Tibshirani, An Introduction to the Bootstrap, Vol. **57**, CRC Press 1994.
[85] S. Pathak, S.-K. Choi, N. Arnheim, M. E. Thompson, Journal of the American chemical Society **123** (2001) 4103-4104.
[86] N. N. Mamedova, N. A. Kotov, A. L. Rogach, J. Studer, Nanoletters **1** (2001) 281-286.
[87] C. T. Dameron, R. N. Reese, R. K. Mehra, A. R. Kortan, C. P. J., M. L. Steigerwald, L. E. Brus, D. R. Winge, Nature **338** (1989) 596-597.
[88] J. D. Holmes, D. J. Richardson, S. Saed, r. Evans-Gowing, D. A. Russel, J. R. Sodeau, Microbiology **143** (1997) 2521-2530.
[89] C. T. Dameron, B. R. Smith, D. R. Winge, The Journal of Biological Chemistry **264** (1989) 17355-17360.
[90] C. T. Dameron, D. R. Winge, Trends in Biotechnology **8** (1990) 3-6.
[91] C. T. Dameron, D. R. Winge, Inorganic Chemistry **29** (1990) 1343-1348.
[92] C. L. Torres-Martínez, L. Nguyen, R. Kho, W. Bae, K. Bozhilov, V. Klimov, R. K. Mehra, Nanotechnology **10** (1999) 340-354.
[93] E. Terpetschnig, H. Szmacinski, H. Malak, J. R. Lakowicz, Biophysical Journal **68** (1995) 342-350.
[94] G. Vereb, E. Jares-Erijman, P. R. Selvin, T. M. Jovin, Biophysical Journal **74** (1998) 2210-2222.
[95] A. Bensimon, A. Simon, A. Chiffaudel, V. Croquette, F. Heslot, D. Bensimon, Science **265** (1994) 2096-2098.

[96] D. Bensimon, J. A. Simon, V. Croquette, A. Bensimon, Physical Review Letters **74** (1995) 4754-4757.
[97] J.-F. Allemand, D. Bensimon, L. Jullien, A. Bensimon, V. Croquette, Biophysical Journal **73** (1997) 2064-2070.
[98] X. Michalet, R. Ekong, F. Fougerousse, S. Rousseaux, C. Schurra, N. Hornigold, M. v. Slegtenhorst, J. Wolfe, S. Povey, A. Bensimon, Science **277** (1997) 1518-1523.